Manufacturing and impact behaviour of aeronautic overmolded grid-stiffened thermoplastic carbon plates

F. Neveu, C. Cornu, P. Olivier, Bruno Castanié

Version of Record: https://www.sciencedirect.com/science/article/pii/S0263822322000411
Manuscript_9db7df4967be452092089c6311cc732d

Manufacturing and Impact behaviour of aeronautic overmolded grid-stiffened thermoplastic carbon plates

F. Neveu [a], C. Cornu [b], P. Olivier [a], B. Castanié [a,*]

[a] Institut Clément Ader (ICA), ISAE, CNRS UMR 5312-INSA-Mines Albi-UPS, Toulouse, France

[b] CETIM, TECHNOCAMPUS EMC2, ZI du Chaffault, 44340 BOUGUENAIS France

* Corresponding author: bruno.castanie@insa-toulouse.fr

Keywords:

Thermoplastic, Carbon laminates, Overmolding, Aeronautics.

Abstract

Thermoplastic composites offer many opportunities for aeronautics. Among them is the possibility of overmolding composite parts to obtain finished "netshape" parts in medium series. This paper presents the complexity of the manufacturing method and the manufacturing defects that may occur in some grid-stiffened overmolded parts using aeronautic thermoplastics. The results of impact tests up to 15 J carried out at various locations of the plates and the grid show that, due to manufacturing defects at the overmolded grid/plate interface, very significant delaminations can be observed.

1. Introduction

Composite structures offer many possibilities for architectures and materials [1], [2], [3]. In the aeronautical field, there is now increased interest in thermoplastic designs that can provide industrial solutions to large series problems [4], [5], [6], [7]. These materials are weldable [7], [8], [9] and easily recyclable. They could also be used in high temperature applications [10]. They have the reputation of being more tolerant than thermosets to damage, which is a sizing point for aeronautical structures [11].

However, this point is still being investigated [12], [13], [14] as it is not perfectly clear – in particular because of unstable crack growth under mode II. Such materials have long been used in the automotive or electronics industries. In particular, they make it possible to obtain "net shape" parts by overmolding, which do not require subsequent machining [15], [16], [17]. Thermoplastics (for example polyamides) are widely used in these industries but offer insufficient mechanical qualities for aeronautical parts [18]. It is therefore necessary to use so-called high performance thermoplastics (PEEK, PAEK, PES, PEI, etc.), which are currently the subject of much research for future industrialization [4], [5], [6].

However, the possibility of overmolding with this type of thermoplastic has been very little studied, from either an academic or an industrial point of view. Recently, in a project whose acronym was "TOAST", a demonstrator of an aircraft airbrake-like structure in modern hybrid design was developed and manufactured [19]. It consisted of a titanium load introduction fitting, a CFRP thermoplastic plate with an overmolded 3D shape under the fitting. In this completely new design, there are no longer connecting elements. A similar study was carried out on “brackets” [20]. From an academic point of view, only one publication reports overmolding with high performance thermoplastics for aeronautics [21]. In [21], simple, straight stiffeners in short-fiber CF/PPS were overmolded with carbon/PPS (carbon fiber / polyphenylene sulphide) laminate plates. In this study, the question was mainly one of characterizing the interface between the overmolded part and the original plate. It appeared that the quality of the interface depended on the design of the stiffener foot (4 configurations tested) and also on the position in relation to the injection flow.

The objective of the work presented here was first to obtain a stiffened specimen having the general shape given in Figure 1. So the important manufacturing issues encountered are shown. As the problem of low speed impact, low energy is the main sizing criterion [11] for aeronautical structures, the overmolded parts were impacted and the damage patterns are analysed here. The specimens have dimensions of 100 mm x 150 mm, which correspond to the standards for impact and post-impact compression tests in the aeronautical industry ([11], Airbus AITM 1-0010 standard). First, the possible

pairs of thermoplastic materials (skin/overmolded grid) will be studied. Then, the problems of manufacturing such parts will be explained. Finally, the results of the impact tests will be presented. Since overmolded composite structures are relatively new, no data have been established concerning this type of test for this type of structure. The following questions are thus unanswered at the present time:

- What is the influence of overmolding on the response of the structure to impact?
- Does the location of the impact change the damage pattern?
- Does the geometry of the overmolding and its orientation in relation to the first ply have an impact on the results?
- What is the influence of manufacturing defects on the impact response?

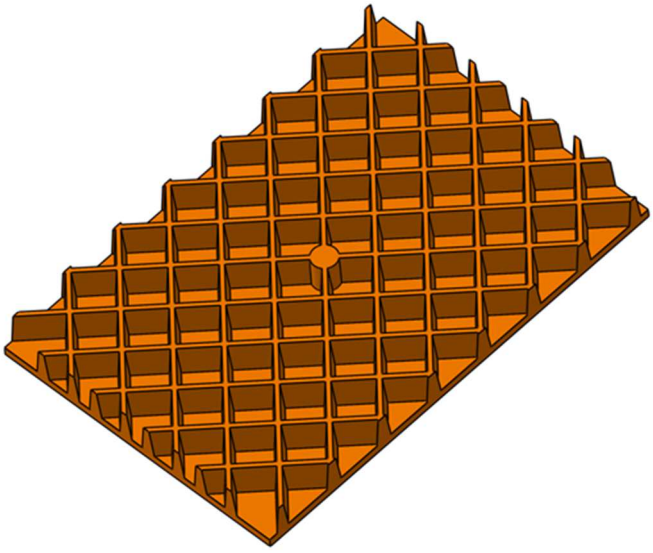

Figure 1. General shape of the specimens to be manufactured.

2. Analysis of the compatibility of the plate and the overmolded grid materials.

2.1 Specimens, Test methods and Materials.

The quality of the bond between the overmolded grid and the plate is decisive for the mechanical strength of the structure. If the bond turns out to be too weak mechanically, a structure with overmolded stiffeners loses much of its interest since the slightest detachment will result in total loss of the stiffening function. Among the factors that can influence the mechanical strength, it is possible to cite a priori:

- Compatibility between the resins of the compound to be injected and the plate
- Injection temperatures
- Compaction pressures and times
- The design of the rib foot
- The distance to the injection point

To determine the mechanical strength of the overmolding, a conventional test mold with tabs, belonging to CETIM, was used for pull-out and unfolding tests. The CETIM mold makes it possible to manufacture composite plates comprising twenty overmolded tabs distributed in four rows of five pieces, as illustrated in Figure. 2. A finished plate is shown in Figure. 3. The injection point is located in the center of the space and the filling is therefore symmetrical (or almost, because each row has a rib foot of different design). The position of each tab relative to the injection site was noted in order to assess whether this factor had any influence on the results.

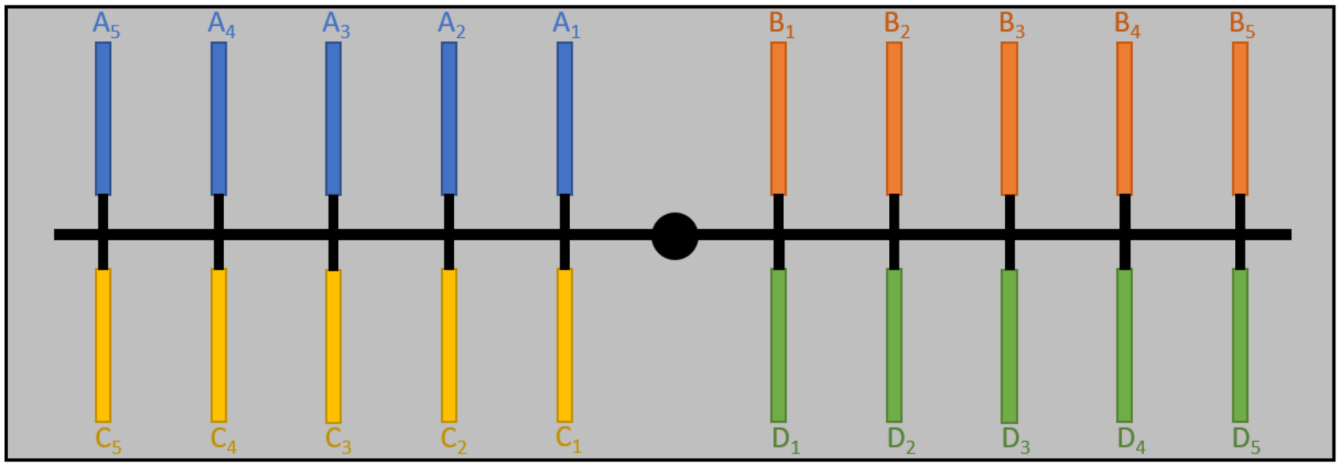

Figure 2. Arrangement of the overmolded tabs.

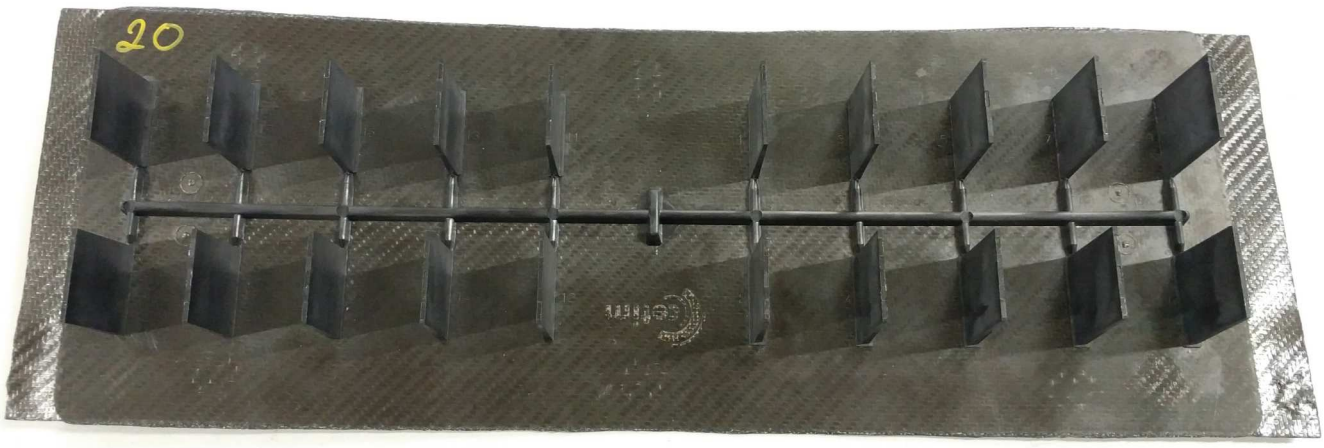

Figure 3. Plate after manufacturing.

The designs of the 4 types of feet are shown in Figure 4:

Without foot (from A1 to A5)

With foot in the form of a "step" (from B1 to B5)

With foot in the form of a small chamfer (from C1 to C5)

With foot in the form of a large chamfer (from D1 to D5)

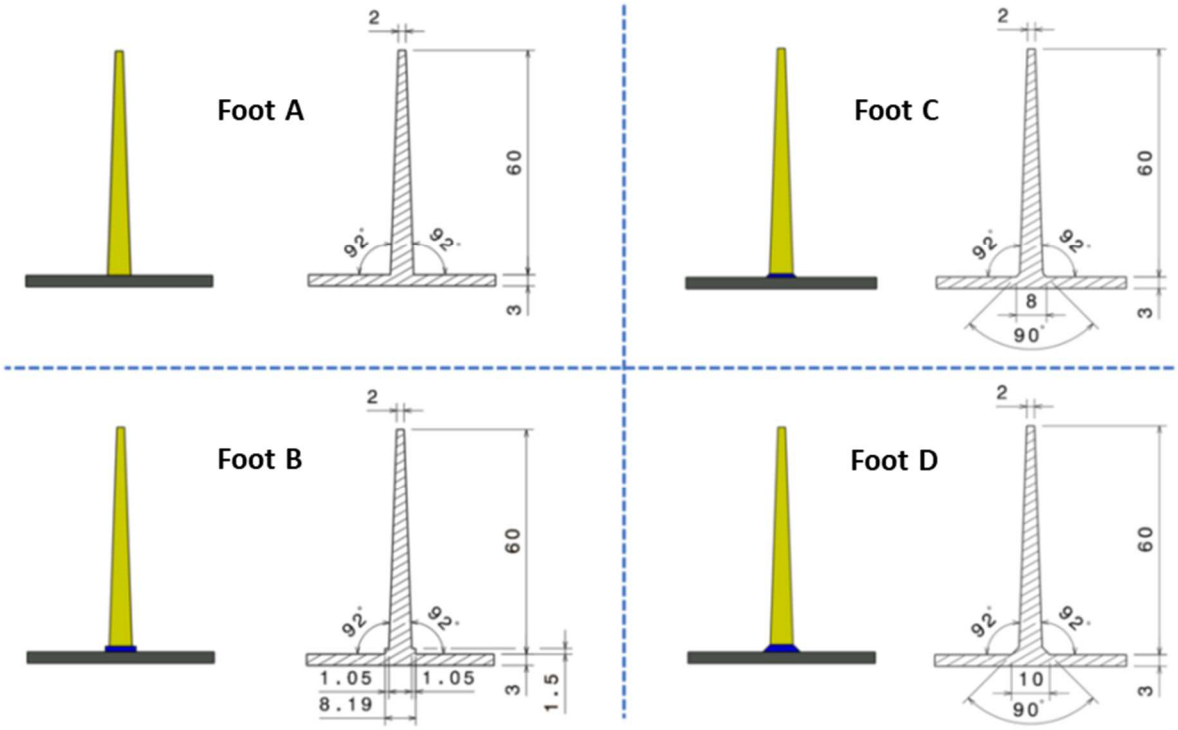

Figure 4. The four designs of the feet of the overmolded tabs.

The twenty specimens per plate were cut on a water jet cutting machine. It should be noted that, despite the precautions taken, some specimens were lost during cutting, which explains some missing samples in the test matrix (Table 1). The specimens obtained after the cutting operations had final dimensions of 60 mm x 50 mm. An overview of these specimens is given in Figure 5. These specimens were used directly on their respective assemblies; only slight retouching was needed when the resin supply channel visible on the side of the tabs was removed.

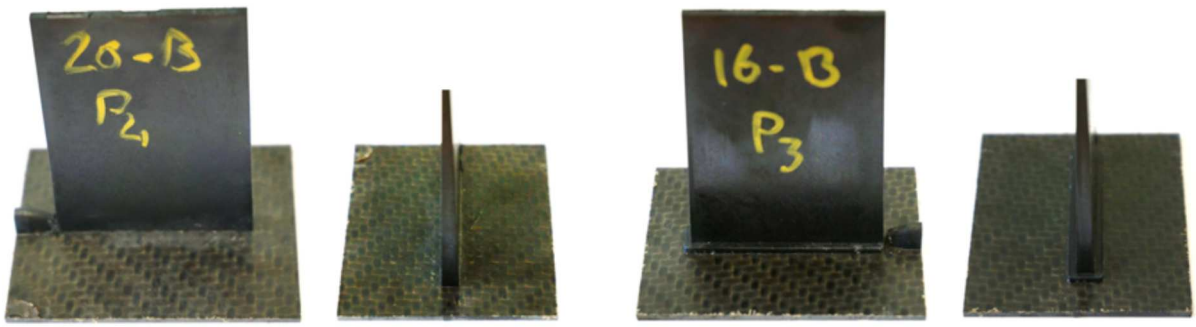

Figure 5. Pictures of the tab specimens (Type A, left; Type B, Right)

An Instron 10 kN type tensile machine was used for the tests because its maximum force is low and the measurement error is minimized. Specific devices were designed for the tab specimens in the two pull-out and unfolding tests. The pull-out test was a simple tensile test in which the jaw of the machine was caught on the tabs. The base of the specimen was kept fixed by the addition of a retaining plate that was screwed over the base of the assembly (Figure 6).

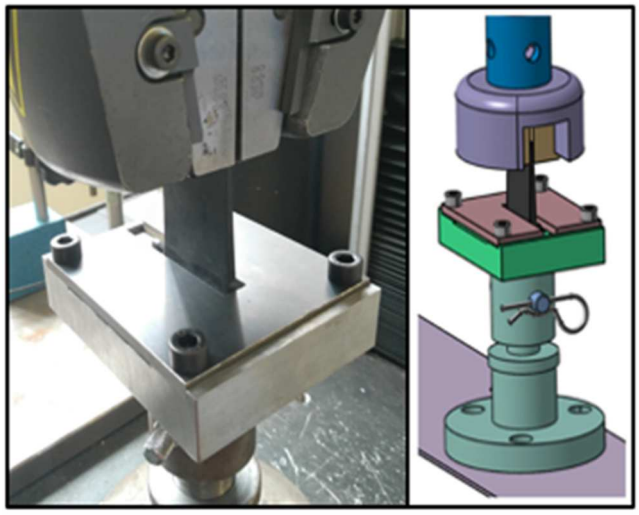

Figure 6. Pull-out (left) and unfolding (right) test setups.

The pairs of materials chosen were consistent with the industrial project to which this study is linked and the test matrix is given in Table 1. Different injection temperatures were tested and the materials are listed below:

Plate

TenCate Cetex PEI, 10 plies $[(0,90)/(\pm45)/(0,90)/(\pm45)/(0,90)]_S$, thickness 3.14 mm

TenCate Cetex TC1100 PPS, 10 plies $[(0,90)/(\pm45)/(0,90)/(\pm45)/(0,90)]_S$, thickness 3.14 mm

Overmolded grid

PPS resin: compound Tedur L9400-1 from Albis (15% ratio of short carbon fibers)

PEEK resin: Victrex PEEK 150 CA30 (30% of short carbon fibres)

It should be noted that a test with PEI resin (Thermocomp EC008PXQ from Sabic) had been carried out but its high viscosity posed injection problems on the overmolded plate (incomplete injection) and this option was abandoned. In the end, 86 pull-out tests and 55 unfolding tests were carried out.

	PEI/PPS 390°	PEI/PPS 410°	PEI/PPS 430°	PPS/PPS	PEI/PEEK
A	5	5	5	5	5
B	5	4	5	4	4
C	-	4	5	5	5
D	0	5	5	5	5

Table 1. Test matrix for tab specimens.

2.2 Results

The force-displacement curves were of the elastic type with a fragile failure and will not be shown here. The results are presented in Tables 2 to 6, which indicate the maximum force measured by the tensile machine as well as the associated normal stress for each configuration of the rib root. Columns 1 to 5 indicate the position of the tab on the original overmolded plate as shown in Figure 2. The mean and standard deviation are calculated for each series of specimens.

							Average	Standard deviation
PEI/PPS 390°		A1	A2	A3	A4	A5	**Foot A**	
	Maximum Force (kN)	0.33	0.39	0.43	0.60	0.63	**0.48**	0.11
	Normal stress (Mpa)	1.92	2.28	2.48	3.51	3.64	**2.76**	0.65
		B1	B2	B3	B4	B5	**Foot B**	
	Effort max	0.14	0.30	0.27	0.18	0.14	**0.21**	0.06
	Normal stress (Mpa)	0.83	1.75	1.60	1.07	0.79	**1.21**	0.37

Table 2. Maximum force and failure stress for the PEI/PPS pair at 390 °C.

							Average	Standard deviation
PEI/PPS 410°		A1	A2	A3	A4	A5	**Foot A**	
	Maximum Force (kN)	0.80	0.93	0.77	0.72	0.67	0.78	0.07
	Normal stress (Mpa)	4.65	5.39	4.50	4.17	3.90	**4.52**	0.40
		B1	B2	B3	B4	B5	**Foot B**	
	Maximum Force (kN)	0.63	0.51	0.38	0.51	-	0.51	0.06
	Normal stress (Mpa)	1.77	1.43	1.08	1.43	-	1.43	0.17
		C1	C2	C3	C4	C5	**Foot C**	

	Maximum Force (kN)	0.14	0.17	0.29	0.42	-	0.25	0.10
	Normal stress (Mpa)	0.45	0.55	0.94	1.39	-	0.83	0.33
		D1	D2	D3	D4	D5	**Foot D**	
	Maximum Force (kN)	0.26	0.34	0.32	0.57	0.39	0.38	0.08
	Normal stress (Mpa)	0.59	0.77	0.74	1.28	0.89	0.85	0.19

Table 3. Maximum force and failure stress for the PEI/PPS pair at 410 °C.

							Average	Standard deviation
		A1	A2	A3	A4	A5	**Foot A**	
	Maximum Force (kN)	0.79	0.88	0.88	1.00	0.79	0.87	0.06
	Normal stress (Mpa)	4.58	5.10	5.11	5.80	4.60	**5.04**	0.36
		B1	B2	B3	B4	B5	**Foot B**	
PEI/PPS 430°	Maximum Force (kN)	0.38	0.42	0.41	0.30	0.36	0.37	0.04
	Normal stress (Mpa)	1.07	1.18	-	0.84	1.02	1.05	0.10
		C1	C2	C3	C4	C5	**Foot C**	
	Maximum Force (kN)	0.30	0.12	0.40	0.36	0.24	0.28	0.08
	Normal stress (Mpa)	0.97	0.39	1.31	1.19	-	0.93	0.27
		D1	D2	D3	D4	D5	**Foot D**	
	Maximum Force (kN)	0.02	0.33	0.44	0.32	0.50	0.32	0.12
	Normal stress (Mpa)	0.03	0.76	0.99	0.72	1.14	0.73	0.28

Table 4. Maximum force and failure stress for the PEI/PPS pair at 430 °C.

							Average	Standard deviation
		A1	A2	A3	A4	A5	**Foot A**	
	Maximum Force (kN)	0.94	0.93	1.13	1.36	0.58	0.99	0.20
	Normal stress (Mpa)	5.46	5.42	6.60	7.88	3.38	**5.75**	1.19
		B1	B2	B3	B4	B5	**Foot B**	
	Maximum Force (kN)	1.46	1.16	-	1.16	1.05	1.21	0.13
PEI/PEEK	Normal stress (Mpa)	4.12	3.29	-	3.26	2.98	3.41	0.36
		C1	C2	C3	C4	C5	**Foot C**	
	Maximum Force (kN)	0.82	0.62	1.13	0.84	0.53	0.79	0.17
	Normal stress (Mpa)	2.70	2.03	3.72	2.74	-	2.59	0.56
		D1	D2	D3	D4	D5	**Foot D**	
	Maximum Force (kN)	1.05	1.06	1.68	1.30	0.68	1.15	0.27
	Normal stress (Mpa)	2.37	2.41	3.81	2.96	1.53	2.62	0.61

Table 5. Maximum force and failure stress for the PEI/PEEK pair.

							Average	Standard deviation
		A1	A2	A3	A4	A5	**Foot A**	
	Maximum Force (kN)	2.19	1.56	1.51	1.59	1.58	1.69	0.20
PPS/PPS	Normal stress (Mpa)	12.73	9.10	8.76	9.27	9.19	**9.81**	1.17
		B1	B2	B3	B4	B5	**Foot B**	
	Maximum Force (kN)	2.08	1.40	-	1.59	1.53	1.65	0.21

	Normal stress (Mpa)	5.87	3.95	-	4.49	4.32	4.66	0.61
		C1	C2	C3	C4	C5	**Foot C**	
	Maximum Force (kN)	1.38	1.14	1.70	1.46	1.12	1.36	0.18
	Normal stress (Mpa)	4.53	3.73	5.58	4.80	-	4.47	0.60
		D1	D2	D3	D4	D5	**Foot D**	
	Maximum Force (kN)	1.98	1.99	2.07	1.42	1.19	1.73	0.34
	Normal stress (Mpa)	4.49	4.52	4.70	3.22	2.69	3.92	0.77

Table 6. Maximum force and failure stress for the PPS/PPS pair.

The tables show no clear influence of the injection position from 1 to 5 unlike in [21],. In order to have a more graphic representation of these results, a histogram comparing the mean values of the forces at failure is proposed in Figure 7, with the margins of error representing the maximum and minimum values of each series. In general, there is a large dispersion for this type of test. There is also a great disparity in the results between the three pairs of materials. The tests clearly show the low resistance of the PEI / PPS pair compared to the PPS / PPS or PEI / PEEK pairs. It is the PPS / PPS pair that offers the best adhesion, which is logical because the overmolding and the plate are of the same nature. Although the design of the rib foot seems to have a certain influence in the case of the PEI / PPS pair, the disparities are less for the other two (if we exclude the type C design, which gives the lowest breaking forces in all cases). For the PEI/PPS pair, it shows clearly that a minimum injection temperature is required to have an efficient bonding strength which would be more likely at least around 410°C.

In this study, it is this pair of materials that will be used – for industrial reasons, which are specified in the following subsection.

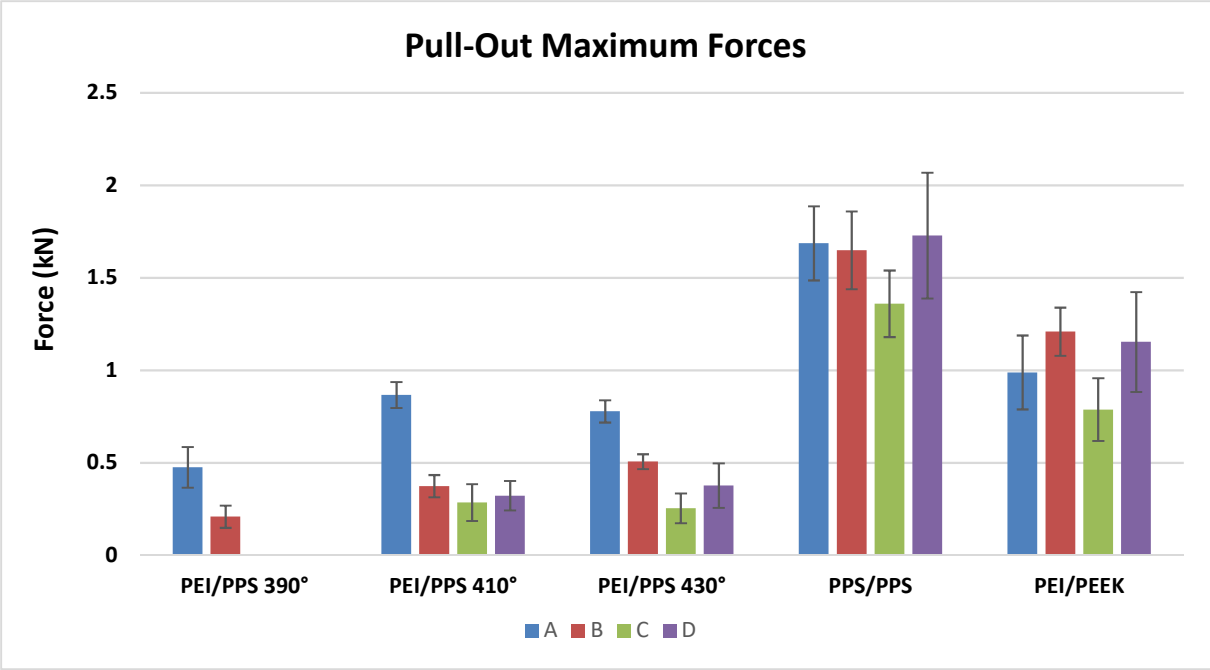

Figure 7. Summary of maximum forces for pull-out tests with standard deviation.

3. Manufacturing issues

Specimen design

The objective was to obtain specimens with dimensions of 100 mm x 150 mm (Figure 1) with an overmolding forming a grid either at 90° or at 45°. After several design iterations, in order to simplify the mold, a larger plate (220 mm x 220 mm) was injected and then cut to obtain the desired shape (Figure 8). There were 4 possible configurations depending on whether the center of the plate on which the impact would take place was located on a corner of the grid or at the bottom of the mesh, at 0° or at 45°.

The chosen material configuration was PEI plate, PPS overmolding. The overmolding was 10 mm high, the thickness of the wall was 2.5 mm and the inner side length of a square was 17.5 mm. To simplify the milling of the mold, a type “A” foot shape was chosen (see Figure 4). Some pictures of the plate before after water jet abrasion cutting and of the specimens after water jet abrasion cutting are also shown in Figure 13.

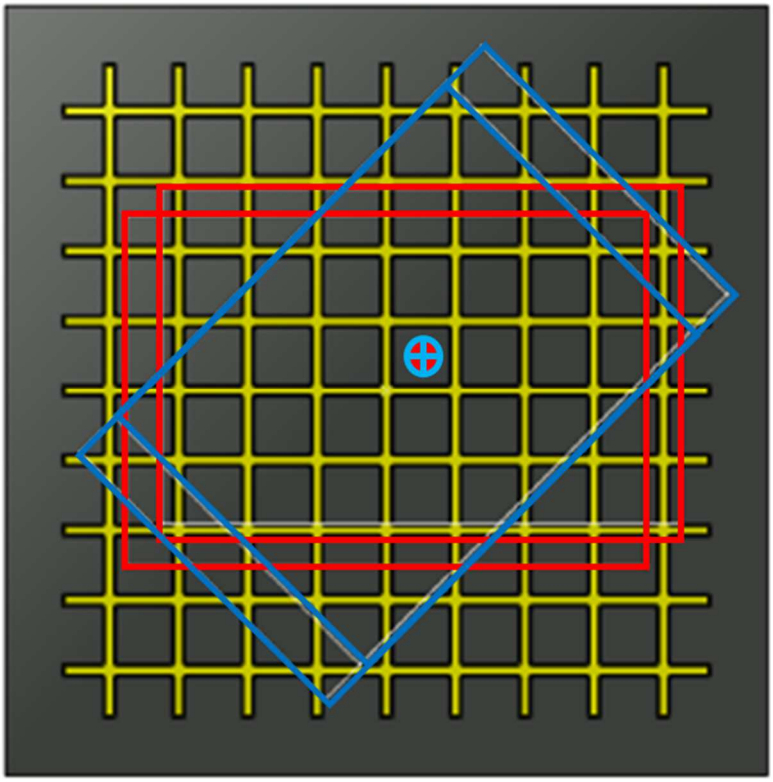

Figure 8. General shape of injected part and specimens cut by water jet.

Mold design

The mold was a very complex part to design and required the expertise of external companies [22], [23] to avoid its being damaged or destroyed by the first injections. It was maintained at a temperature of around 200°C during the injection phase. The CETIM press used allowed the compound to be injected up to a pressure of 1890 Bars. MODFLOW simulations had shown that, with PPS and with two injection points, a pressure of around 200 bars was sufficient to allow injection without defects, with an injection time of less than 1 s. Note that, with a PEI-based compound, the pressure would have risen to 650 bars with a doubled injection time, which could cause problems on real industrial parts. The mold consisted of 7 main parts made of steel and fibreglass (Figure 9): 1: Upper support; 2: Upper mold plate (the grid is machined in); 3: molded part; 4: lower mold plate (the plate shape is machined in); 5: isolating plate (fibreglass); 6: hot injection block; 7: Hot device plate; 8: Lower support.

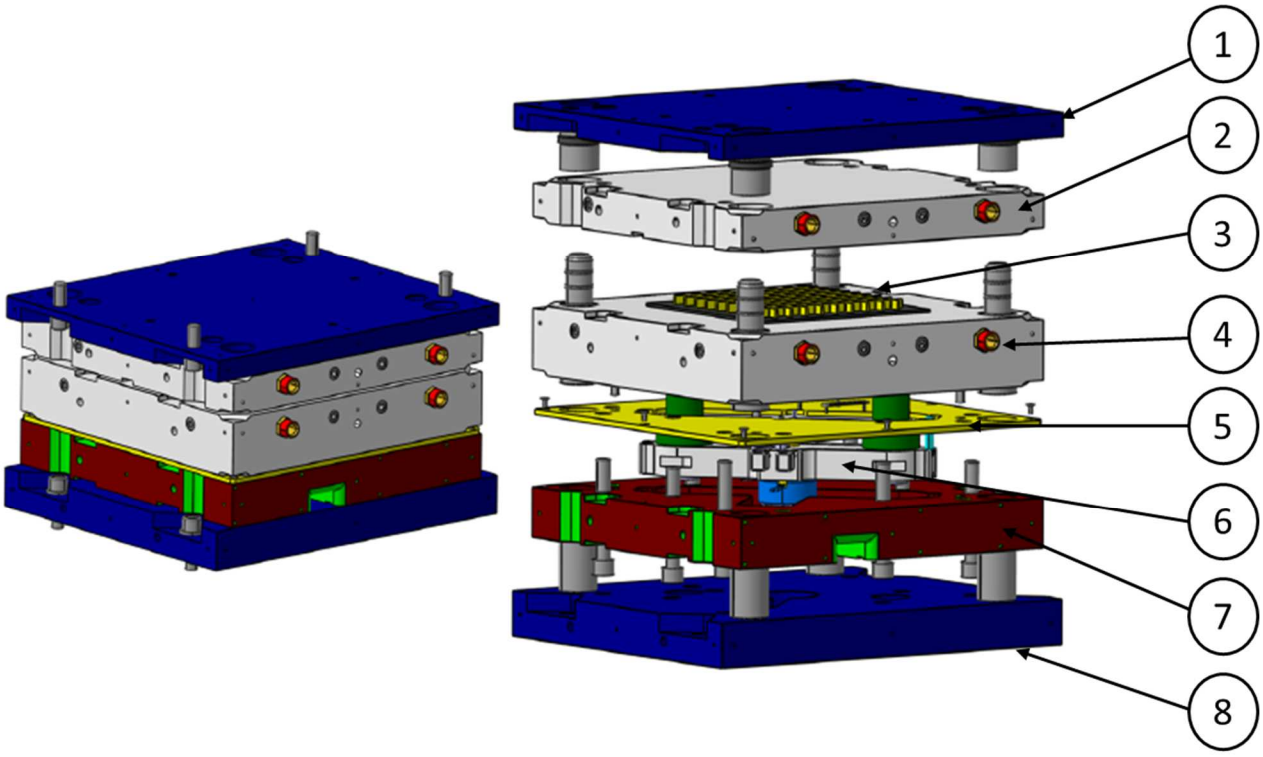

Figure 9. Structure and main parts of the mold.

The upper parts 1 + 2 move and are linked to the upper part of the injection molding machine. They are centred on the lower mold by 4 bushings. Plates 2 and 4 (in grey) are machined to integrate an oil circuit that maintains the temperature of the mold so that the cavity of the grid is hot enough to avoid the injected material undergoing thermal shock during its injection. CETIM has the necessary facilities to implement this type of heating, which is more practical than the use of heating rods. Among the peculiarities of plate 4, two notches were also machined so that a blade could be slid under the composite plate to facilitate demolding should the injected plate get stuck in the cavity when the mold was opened after injection. In fact, this proved to be very handy as the plate remained stuck in about 75% of the cycles.

The use of two injection points has a direct consequence on the design of the mold since it is necessary to provide additional equipment for integration into the heart of the mold to make it possible to separate the incoming injection channel into two channels feeding the two injection nozzles. This equipment is known as a “hot block”, and specialized companies design and manufacture such products [22], [23]. The hot block is itself a complex piece of equipment and, for large series, it is preferable to have a hot

block optimized and designed specifically for the desired application. This obviously depends on the material injected, the number of injection points and the desired surface finish, which has an impact on the types of nozzles used. The hot block requires special installation in plate 6 and a specialist must travel to carry out its installation and adjustments.

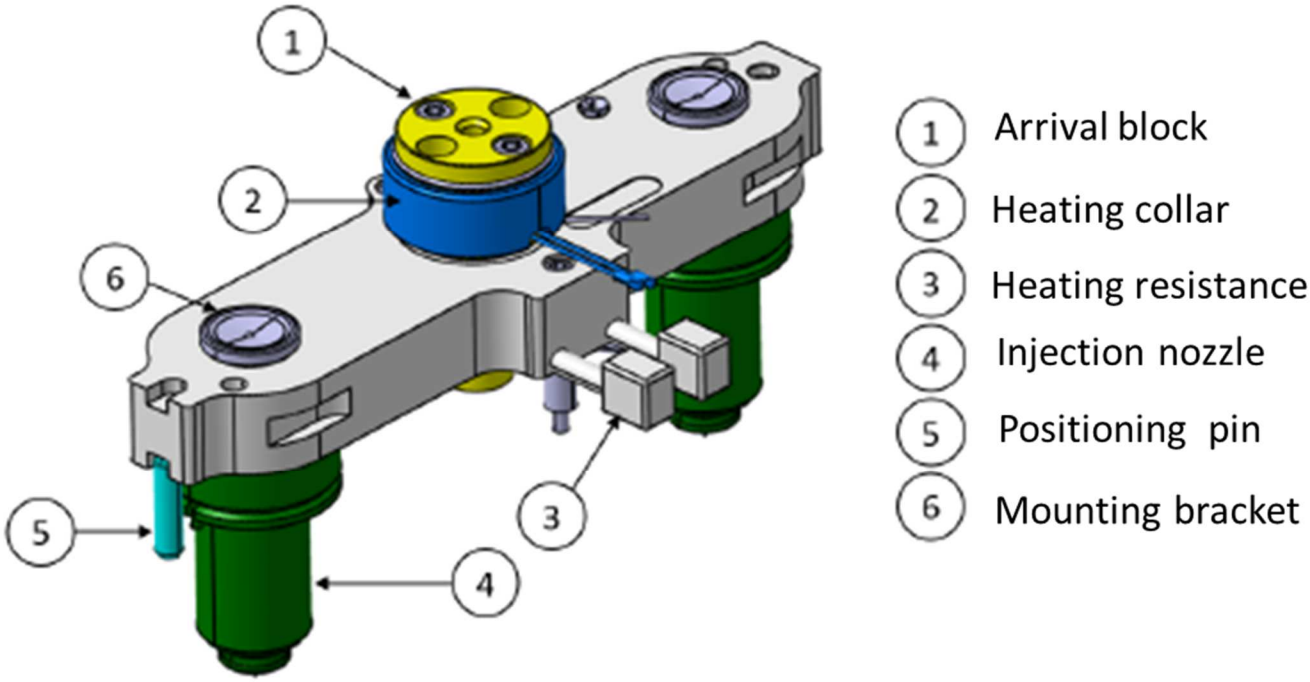

Figure 10. Hot block structure.

Insulating plates are essential for safety reasons. Mainly composed of glass fibers and epoxy, they help to contain the heat within the mold and thus provide protection for the press operators. The mold is therefore entirely streamlined by these insulating plates. An insulating plate (5, figure 9) has also been added between the lower mold plate (4) and the hot block and its support plate (6). This isolates the hot block from the heating oil circuit and also limits the spread of heat to the bottom plate of the press. Note that this plate is much more resistant in compression than standard outer plates since it must withstand the forces introduced by the press during injection. Figure 10 shows the complete mold equipped with

the insulating plates. All in all, the development of the mold required around 6 months of work at a cost of around 20 k€ for machining, various parts, and the cost of technical assistance.

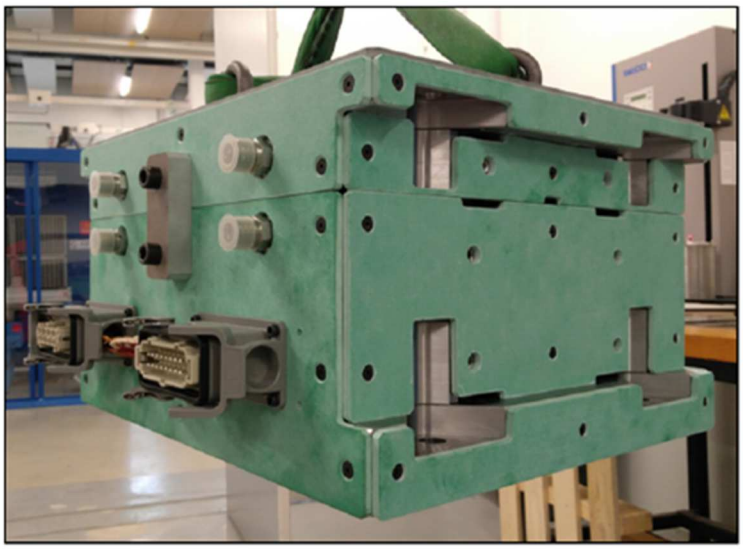

Figure 11. Exterior view of the injection mold equipped with its insulating plates.

Manufacturing of specimens

The entire manufacturing process is divided into several stages, which are essentially composed of periods of transfer, heating and injection. The thermocompression line installed at CETIM thus comprises a conduction furnace, an infrared furnace, a vertical press equipped with its injection unit and a robot for transferring preforms between these different items. The process is illustrated in Figure 12. The steps take place successively as follows:

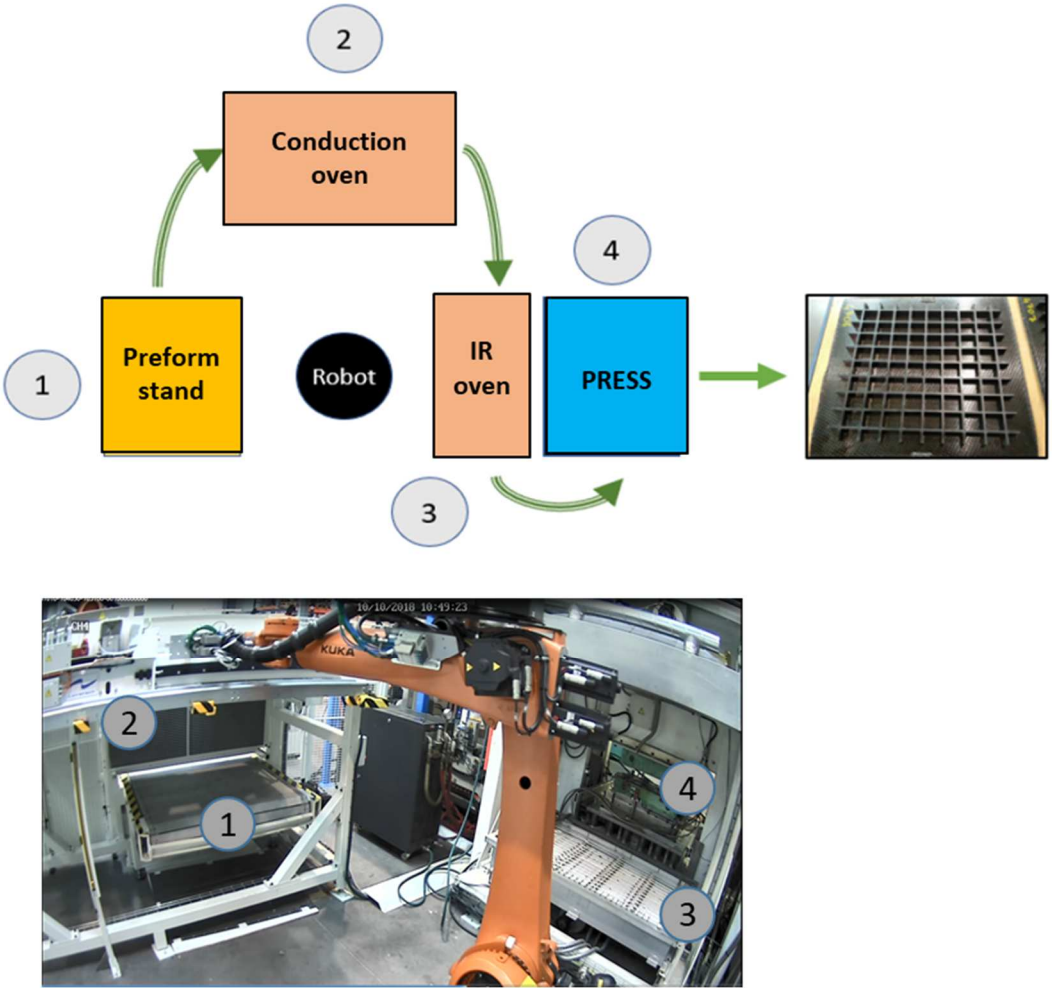

Figure 12. Operating diagram of the thermocompression line and overview of equipment.

1st step: The pre-cut composite preform is placed on the starting stand. In our case, the dimensions of the preform were 220 mm x 220 mm and were chosen because, on the one hand, they allowed post-manufacturing cuts to be made and, on the other hand, they offered a sufficient surface area to have a satisfactory joint plane when the preform was placed on the press during the overmolding phase. These dimensions also correspond perfectly to the overall dimensions of the Tencate plate, thus minimizing the quantities of scrap after cutting of the preforms.

2nd step: The preform is brought into the conduction oven using a gripping hand (denoted robot in Figure 12) made up of suction cups and needles specially adjusted for the preform. At this stage of the process, the preform being in solid form, it is the suction cups that allow its transport to the conduction furnace. Once the

preform has been placed in the oven, a first heating cycle is initiated, the objective being to uniformly heat the preform both on the surface and in the thickness. In our case, this cycle lasted 40 seconds and reached a temperature of 220°C. The melting temperature of PEI is 310°C according to data from the manufacturer, Tencate.

3rd step: A second transfer step is then required to bring the preform from the conduction oven to the infrared oven. The infrared oven has a heating set point of 390 °C, a temperature higher than the melting temperature of the PEI. This higher set point is justified by the fact that the preform is not made of PEI only; all the carbon fibers also need to be heated. In addition, it is important that the preform should come to a state as close as possible to melting when it is placed in position on the press for the injection step. The mechanial bond will be all the more robust if the two resins concerned (that of the preform and that injected for the overmolding) are both molten as the miscibility between them will obviously be improved. It is therefore necessary to anticipate that the preform will move away from the melting point as soon as the infrared oven is opened for the last transfer step. The time planned for this heating period is 80 seconds.

4th step: The last step is the stamping and overmolding. The CETIM installation consists of a 500 tonne press coupled with a 2000 bar injection press. The gripping hand carries out the last transfer from the infrared oven to the press. The distance between the two devices is reduced to a strict minimum to respond to the problem explained above. The needles of the gripping hand are suitable for gripping the preform here since it is in a very viscous state but not liquid. Once the preform has been placed on the mold, the injection cycle begins: the press (and therefore the mold) is closed and the injection unit injects the PPS. At closing, pressure is of the order of 300 bars and the injection temperature of approximately 300 °C. This injection phase lasts for approximately 7 seconds and is followed by a maintenance phase of approximately ten seconds. At the end of this process, the press rises and the overmolded plate can be extracted from the mold (see Figure 13). This plate is then cut with a water jet according to the diagram in Figure 8 to make the impact test pieces (see Figure 14).

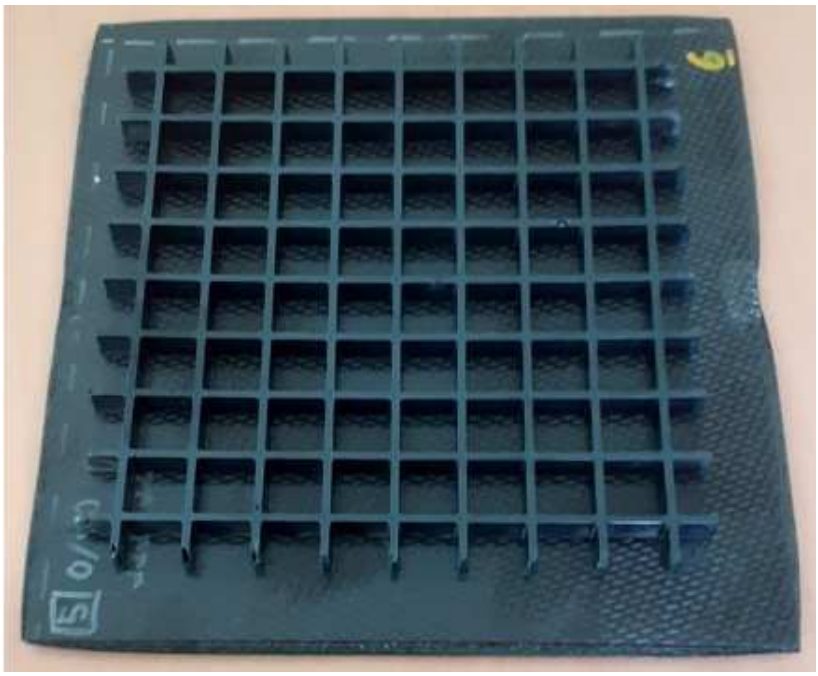

Figure 13. Manufactured plate after injection.

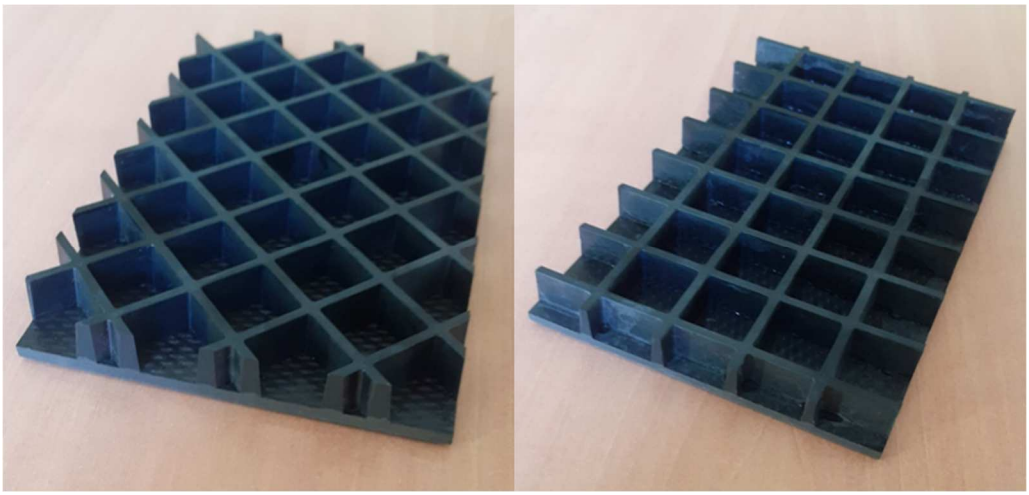

Figure 14. Specimens for impact testing.

Visible defects after manufacturing

For all plates manufactured under normal injection conditions, no bonding defect between the overmolding and the plate was observed. Regarding the injection itself, occasional burning phenomena were found (see Figure 15) on the ends of the injection grid and sometimes in the middle of certain ribs. These were due to the formation of small gas pockets in the mold cavity during injection, into which the resin was unable to penetrate. While these defects were not considered worrying when they were located at the ends of the ribs, the situation was different for those present in the middle of a rib, since a structural weakness was clearly present. However, there were

generally only two burns, at most, per plate produced and their position varied. When the plates were cut to match the dimensions of the impact specimens, the ribs sometimes separated slightly from the composite plate (only for certain injection conditions). This gave us a first clue about the fragility of the overmolding when a non-ideal set of parameters is used. In addition, during these cuts, it was also noticed that some ribs were not completely filled, betraying the presence of gas pockets that Moldflow did not detect during the simulations.

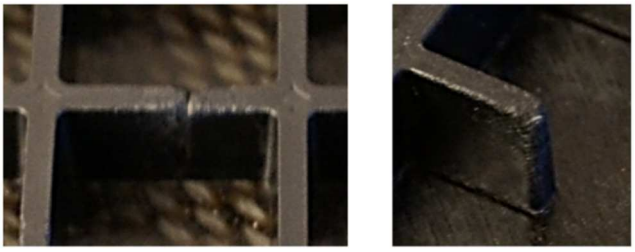

Figure 15. Example of a burn-type defect observed towards the center of the grid and at one end.

Another defect observed was the misalignment of the preform relative to the ribs. This meant, for example, that, in the case where a plate oriented at 0° was used, the ribs, which were supposed to have a direction parallel to the fibres of the preform were actually at an angle to them. In the majority of cases, the shift was less than 5° but, in some cases, an angle of around 30° could be detected, based on visual observations only. This shifting was caused by the gripping hand which, to release the preform on the mold, had to retract its needles. In certain random cases, this operation caused the preform to rotate on itself when it was deposited on the mold, thus resulting in the shift. The potential consequences of this defect on our impact tests seem very limited but would have been quite different in the case of post-impact compression tests. There is also a spring-back effect [26] on the overmolded plates, while the original plate is perfectly flat. This effect is significant and of the order of several mm. It will have to be taken into account for industrial parts, possibly with a compensated mold [27], and investigations on manufacturing simulations remain to be carried out, as for thermosets [28], [29].

Tomography analysis of defect after manufacturing.

The poor impact results presented in the next paragraph led us to look more closely at the interface between the molded part and the plate by carrying out a tomography analysis on remaining pristine plates. In fact, there were many, sometimes very significant, defects. A local undulation of the upper layers of the plate was systematically observed in line with the ribs. In the extreme case presented in Figure 16, enormous porosity and fiber breaks were found. In other cases, the injected resin was also seen to raise the adjacent layers. Clearly, these defects, which had not been observed on the tab test pieces, weakened the impacted specimens.

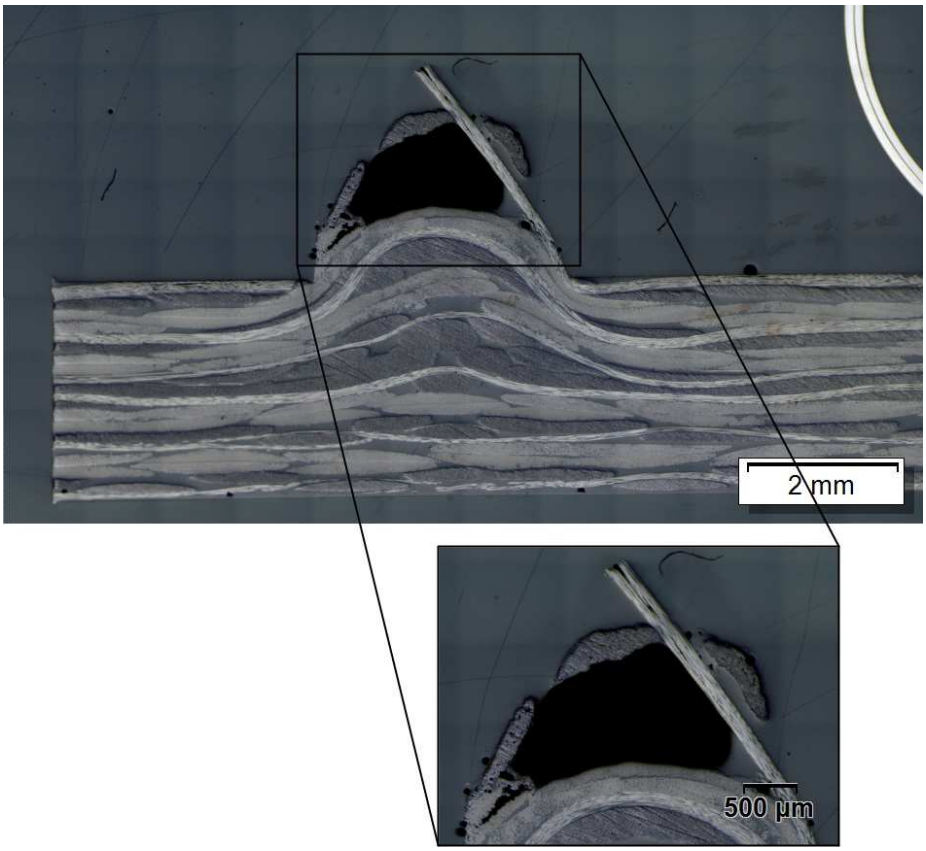

Figure 16. Cross-section of carbon-PEI laminated plate after a stage at PEI melting temperature in the injection mold.

4. Impact Behavior

Method

The tests were carried out with a falling weight, which has already been described several times in previous publications, as has the measurement methodology [11], [24], [30]. A hemispherical impactor 16 mm in diameter enabled an impact test to be performed inside a square of the grid. To limit the number of tests and specimens, only two possibilities of impact were chosen:

- Between the ribs, directly on the laminate
- On a crossing of ribs

It was also important to study the impacts on the non-overmolded side of the composite plate because, depending on the design, the ribs may or may not be visible. For this reason, the impact tests were carried out on both sides of the overmolded plate at the two locations mentioned above. For clarity, Figure 17 summarizes the four front and back impact locations, for 90° and 45° grids. The color conventions and continuous lines (90° grid)

or dotted lines (45° grid) are kept for the test curves. Reference tests were also carried out on non-overmolded plates to determine the BVID (Barely Visible Impact Damage). Consequently, to remain in the damage tolerance domain, the impacts were at 5, 10 and 15 J, with one plate per configuration, i.e. a total of 8x3 = 24 tests.

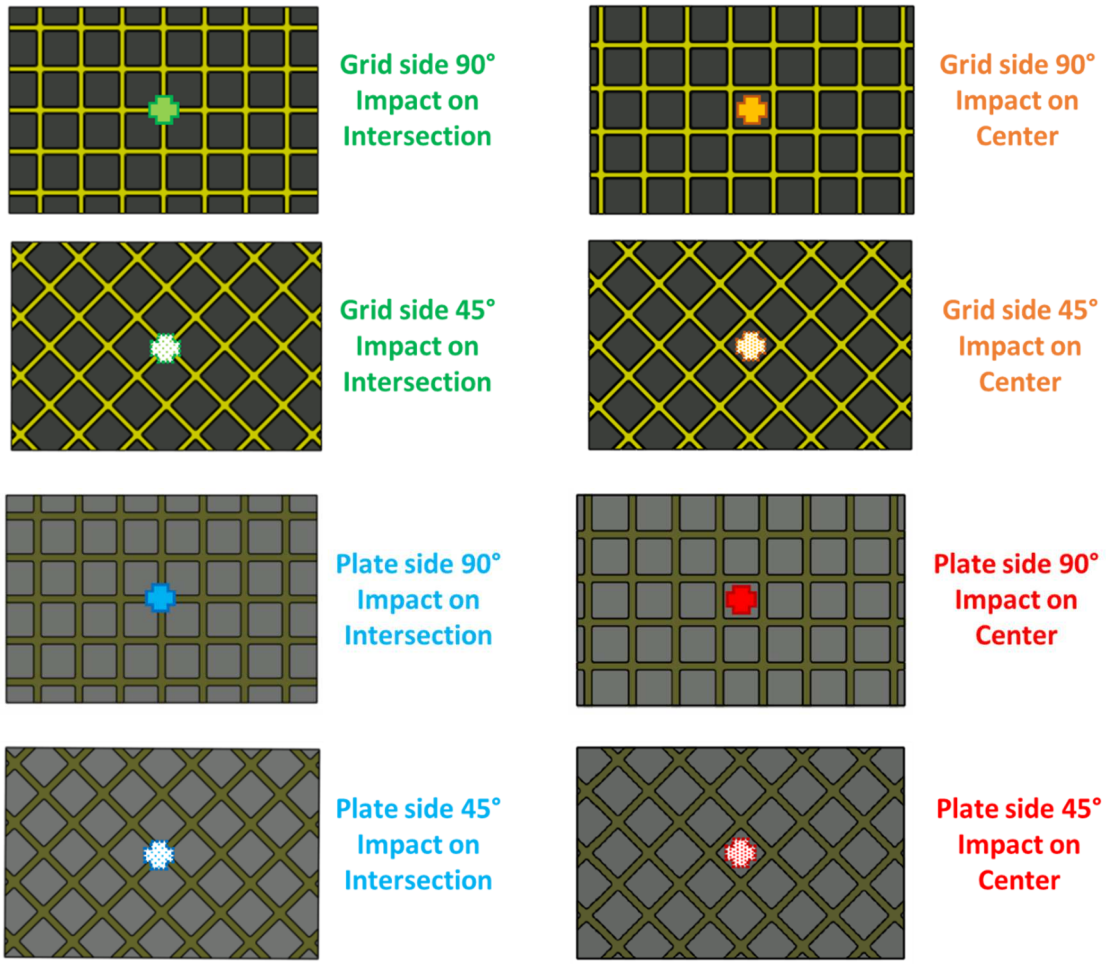

Figure 17. The 8 impact configurations.

Looking for BVID

Five tests were carried out, at 5, 10, 15, 20 and 25 Joules, on Tencate specimens 100 x 150 mm^2 without overmolding following the method described in [11] or [30]. The displacement force curves are given in Figure 18. A first contact zone of 0.5 mm is noticeable, followed by an almost linear rise, which is noisy because of the dynamics of the impact, then a change in slope linked to the creation of damage in the plate. These curves are very similar to those of Vieille et al. [12] although the thermoplastics are different (PEEK and PPS). The contact zone may be connected with a phenomenon of clearance linked to the plate/assembly contact due to plate springback. The change in slope is attributed to the beginnings of fiber breakages at 90° and 0° [12], which then multiply. The measurement of the residual indentation, due to the relaxation effects, was carried out more than 72

hours after the impact test. The measuring device was an Alicona Infinite Focus SL which is an optical 3D measuring system. A measurement time of 20 minutes per specimen was chosen as the best compromise between time spent and precision. The results are presented in Figure 19. The BVID being set at 0.3 mm in the case of a detailed inspection [25], the threshold energy is was 17 J. To assess the damage tolerance of these structures, tests could be performed at 5, 10 and 15 J. The curves obtained will also serve as a reference with respect to the impacts on the overmolded structure.

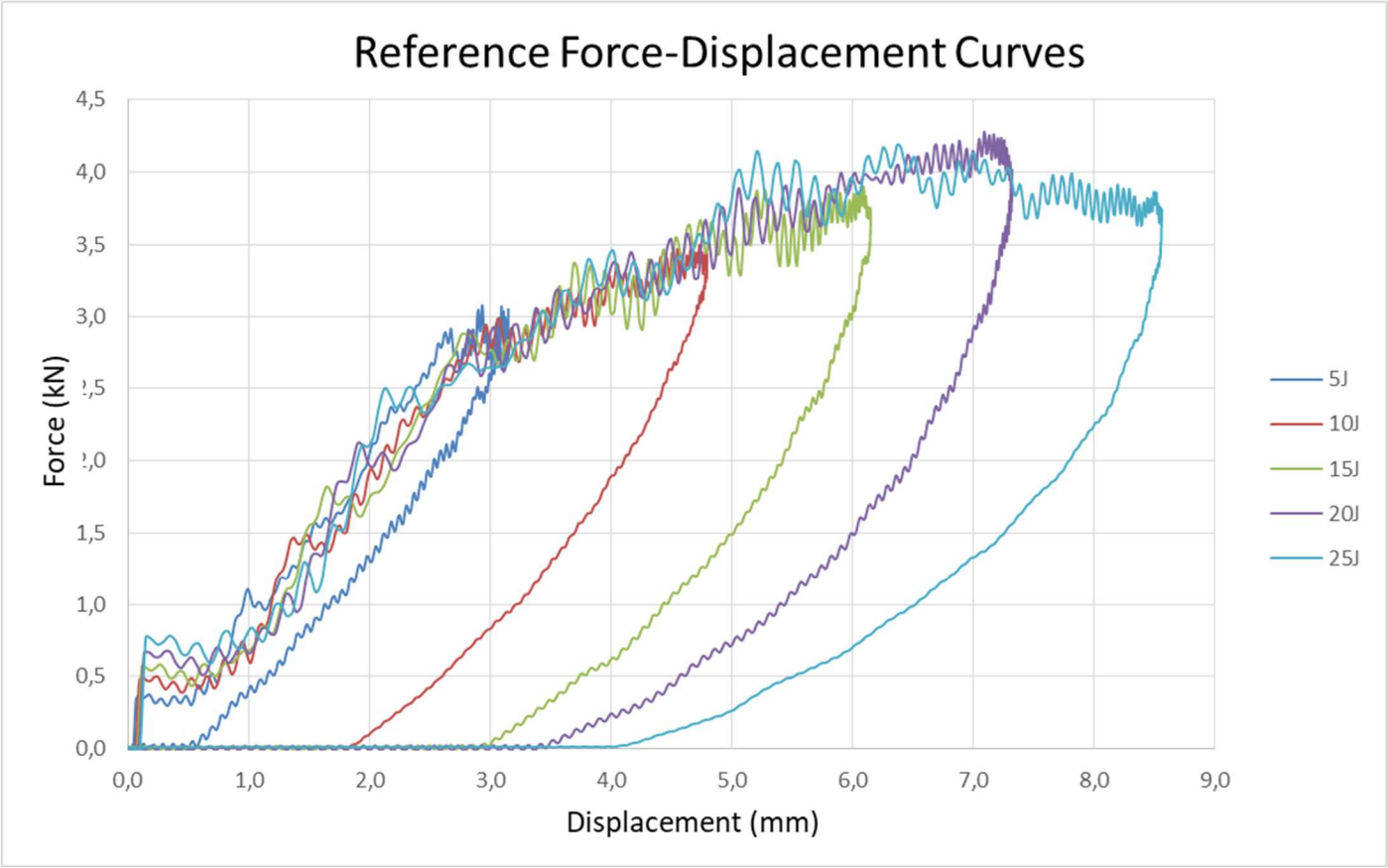

Figure 18. Force-displacement curves for impact tests on Tencate PEI plates without overmolding.

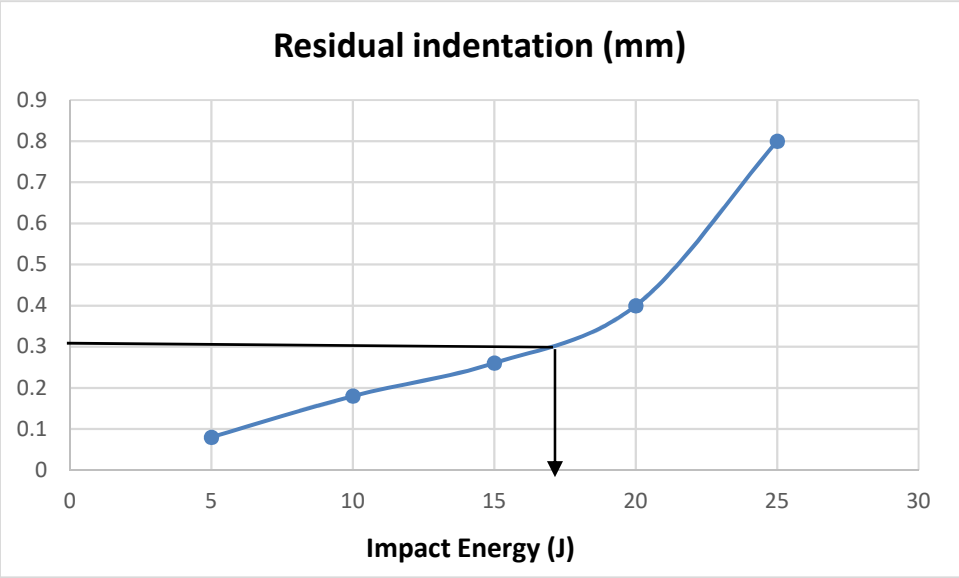

Figure 19. Looking for BVID.

Figure 20 shows the tomographic images in sectional view and centred on the impacts of the reference thermoplastic plate impacted at 10 J, 15 J, 20 J and 25 J. It is interesting to note that, from 10 J, the plate has matrix cracks and a beginning of delamination on the opposite side to the impact. The damage gradually intensifies as the impact energy increases. From 15 J, fiber breaks are visible on the face opposite the impact. From 20 J, the impact zone can be judged to be considerably damaged. At 25 J, the damage has spread throughout the thickness of the plate and is close to perforation. These modes of damage are, of course, always present with overmolded plates.

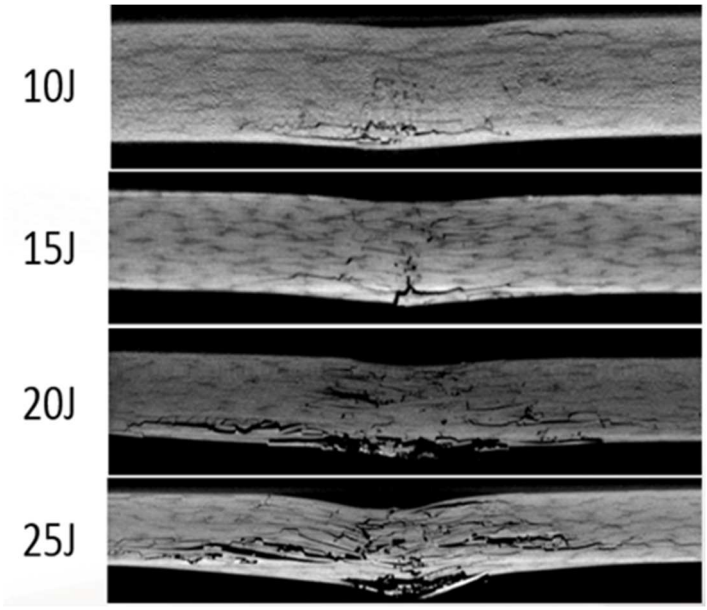

Figure 20. Tomography of damage on non-overmolded plate.

Post impact visible patterns on overmolded grid

The main types of damage qualitatively observable with the naked eye on the overmolded grid are shown in Figure 21. In the first photo, cracks are visible in the ribs of the grid. In the second photo, it is clear that the grid has separated from the plate. The photo shows one side of the plate but these cracks are of the same nature in the center of the plate. Note that the failure does not occur quite at the foot of the rib (at the geometric level of the rib/plate interface but slightly higher). Corrugations in the plate are clearly visible at this point and it appears that part of the plate has been pushed into the cavity of the grid as already shown in Figure 16. Therefore, the breakage still occurs at the interface of the two thermoplastics. In the third photo, the impact was very strong and an area of the grid broke and became detached.

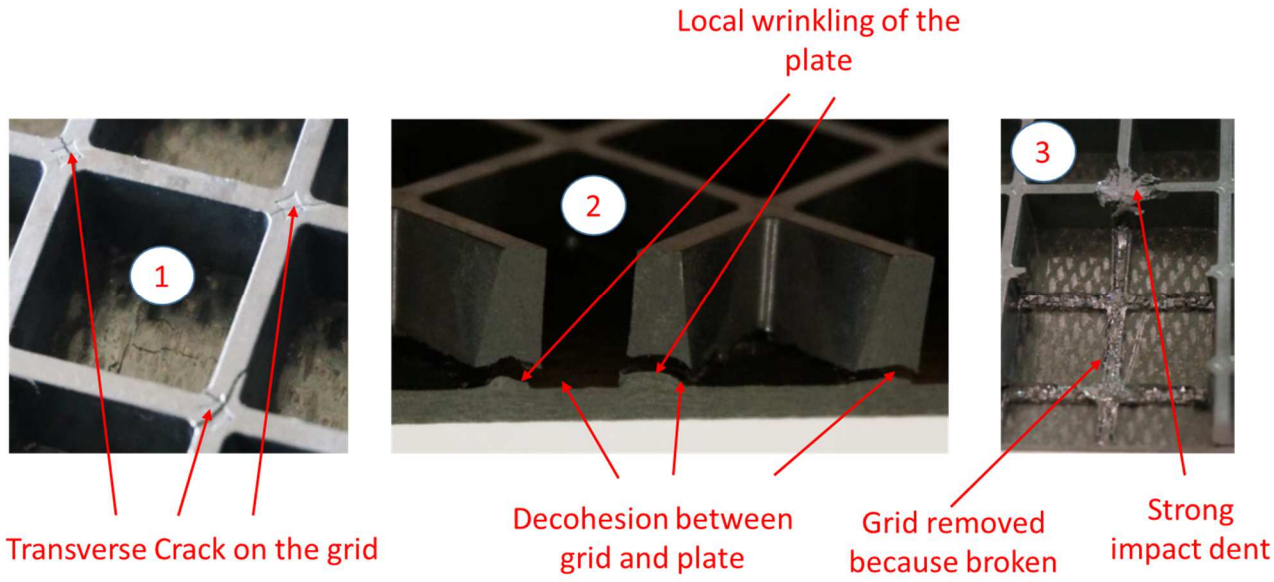

Figure 21. Type of damage on the overmolded grid.

Table 7 gives a summary of the damage. If we concern ourselves with the behaviour of the plate alone, the influence of the grid is globally weak, except in the case of impact on the plate side to the right of a grid intersection. In this case the damage is, with one exception, limited even for 15 J. This case is logically favourable because the material of the grid facing the impact zone limits the bending and localizes the compression. In all the other configurations and for 80% of the cases, a significant grid/plate delamination is observed, even for the tests at 5 J. It is clear that, from this point of view, the overmolded solution, although it allows self-stiffening technological solutions and "net shape", does not make any contribution to damage tolerance. This behavior can

be explained, not only by the low toughness of the PEI/PPS interface as demonstrated in the previous section, but also by the fact that thermoplastics are sensitive to velocity effects in mode II [14], which results in the occurrence of very large delaminated areas in certain configurations. In general, it seems that the 45° grids are more damaged than the 90° grids. Some cases are exceptions in both directions, so it is possible that there are variations in manufacturing, which will be shown in the following sections.

Impact Energy	Grid direction	Impact Side	Impact Location	Dent on impact side	Dent on opposite side	Crack on grid	Grid/plate decohesion percentage	Absorbed Energy (J)
5J	90	Grid	Intersection	slight	no	yes	10%	2.64
5J	45	Grid	Intersection	slight	no	no	no	2.73
5J	90	Grid	Centre	yes	yes	no	no	3.01
5J	45	Grid	Centre	slight	slight	no	60%	2.31
5J	90	Plate	Intersection	no	no	slight	no	2.28
5J	45	Plate	Intersection	slight	no	yes	60%	1.74
5J	90	Plate	Centre	yes	slight	yes	10%	2.97
5J	45	Plate	Centre	slight	no	yes	10%	2.49
10J	90	Grid	Intersection	slight	no	yes	30%	7.04
10J	45	Grid	Intersection	slight	no	yes	60%	7.04
10J	90	Grid	Centre	yes	yes	no	60%	6.96
10J	45	Grid	Centre	yes	yes	no	80%	6.79
10J	90	Plate	Intersection	yes	no	yes	10%	7.25
10J	45	Plate	Intersection	yes	no	yes	no	6.87
10J	90	Plate	Centre	yes	slight	yes	10%	3.21
10J	45	Plate	Centre	yes	slight	yes	10%	6.77
15J	90	Grid	Intersection	deep	Yes	yes	Grid Broken	14.29
15J	45	Grid	Intersection	X	X	X	Grid Broken	14.33
15J	90	Grid	Centre	yes	yes	no	80%	X
15J	45	Grid	Centre	yes	yes	no	100%	11.36
15J	90	Plate	Intersection	yes	no	yes	no	11.38
15J	45	Plate	Intersection	yes	no	slight	10%	10.62
15J	90	Plate	Centre	yes	yes	yes	10%	11.67
15J	45	Plate	Centre	yes	yes	yes	10%	X

Table 7. Overview of damage modes

Force / displacement curves for 5 J impacts.

The displacement force curves for an impact at 5 J are given in Figure 22 for the molded grid side, and in Figure 23 for the plate side. Globally, for the plate side impacts, the response appears identical, the contact phase is similar and is probably due to the curvature of the plate generated by the springback. The energy absorbed for the reference plate is 1.64 J and for the overmolded plates it is higher, oscillating between 1.74 J. and 2.97 J. The

maximum delamination is reached for the minimum absorbed energy, which suggests that the debonding occurred early and consumed little energy. It could therefore be a manufacturing defect. However, in this case of early debonding, there is thus a contribution of the grid to the energy absorption and the grid is also damaged. In the case of the impact on the overmolded grid side, there is a significant difference in behaviour according to whether the impact is on the grid or at the bottom of a square. The energy absorbed is greater and varies from 2.31 J to 3.01 J, the minimum being obtained for the same configuration as before, with a debonding of 60% of the grid. There is no longer a contact zone and the initial slopes are greater, which is logical given the contribution of the grid to the bending. The maximum contact forces are also increased relatively to the reference plate when the impact falls directly on the grid. In this case, the damage is minimal and the grid does play a protective role. On the other hand, during an impact at the bottom of a square, especially for the 90° case, the signal is very noisy, which probably corresponds to the grid/plate debonding up to 60% as noted. However, this phenomenon is not present for the plate with a 45° grid, which shows more similarity with the impact on the reference plate.

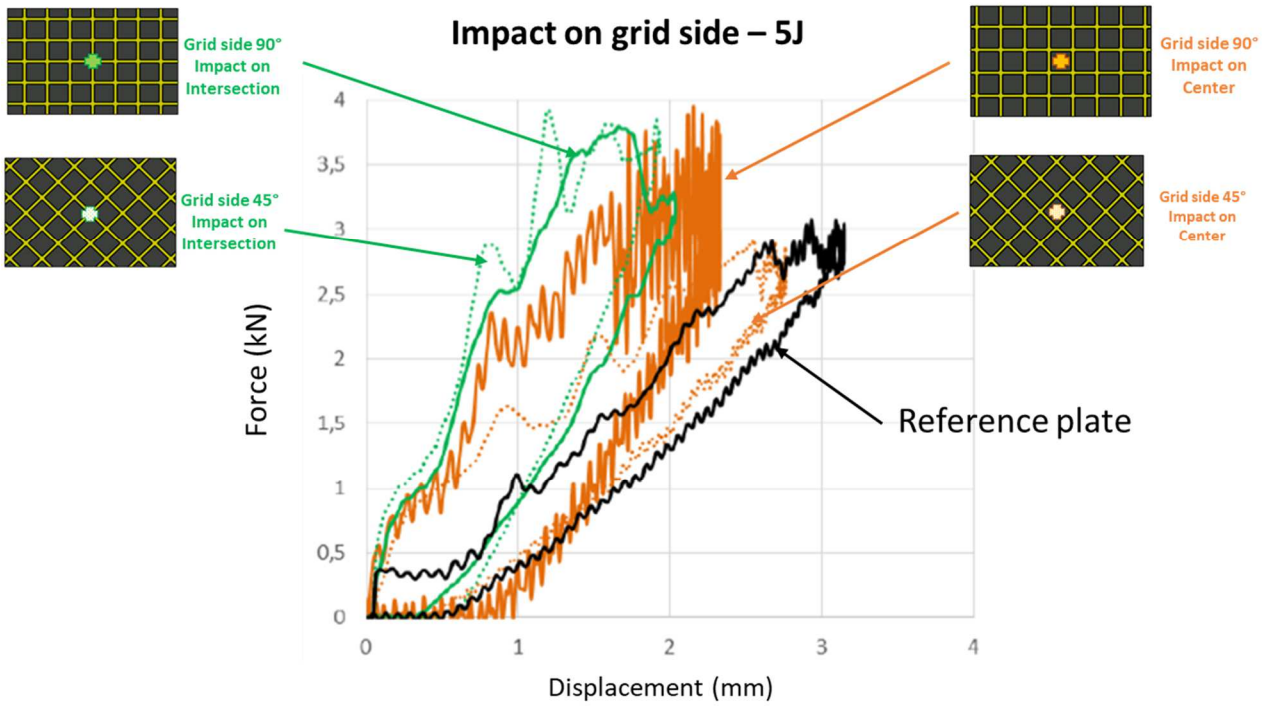

Figure 22. Displacement force curves for an impact at 5 J, overmolded grid side.

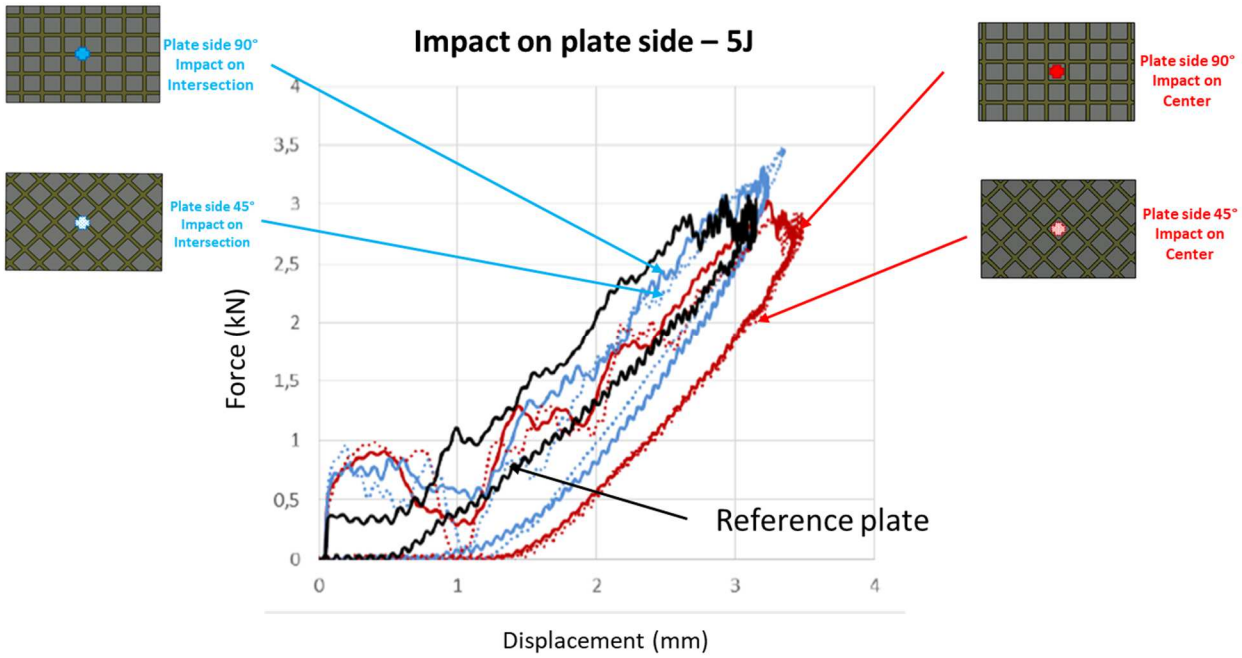

Figure 23. Displacement force curves for an impact at 5 J, plate side.

Force / displacement curves for 10 J impacts.

Figure 24 gives the force/displacement curves for an impact at 10 J on the overmolded grid side and Figure 25 gives them for the plate side. Globally, the same trends as with 5 J are observed. For the plate side impacts, the energy absorbed from the reference plate is 6.07 J and, here, the energies range from 6.77 J to 7.25 J with an aberrant point at 3.21 J. For this test, it appears probable that the impactor was badly centerd on the mesh. For impacts on the grid side, the absorbed energies are 7.04 J for the impact on an intersection and 6.79 J and 6.96 J for an impact at the bottom of the mesh, which become comparable to the impacts on the plate side in terms of response. The damage, although greater, is also limited when an intersection is impacted.

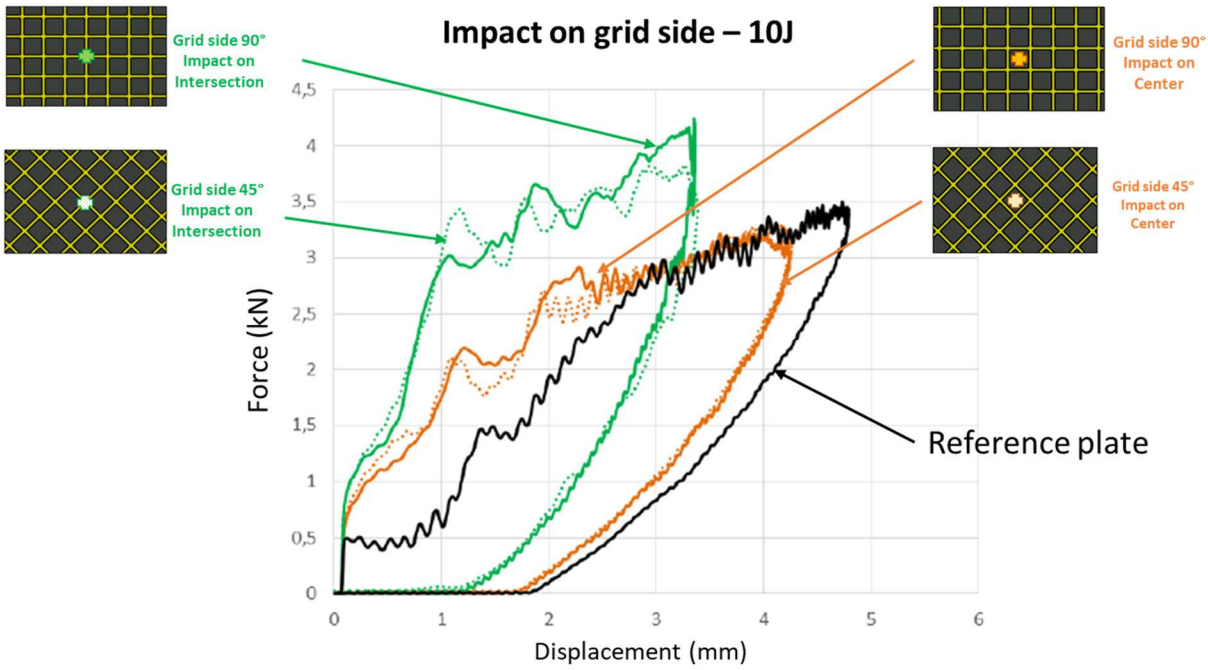

Figure 24. Displacement force curves for an impact at 10 J, overmolded grid side.

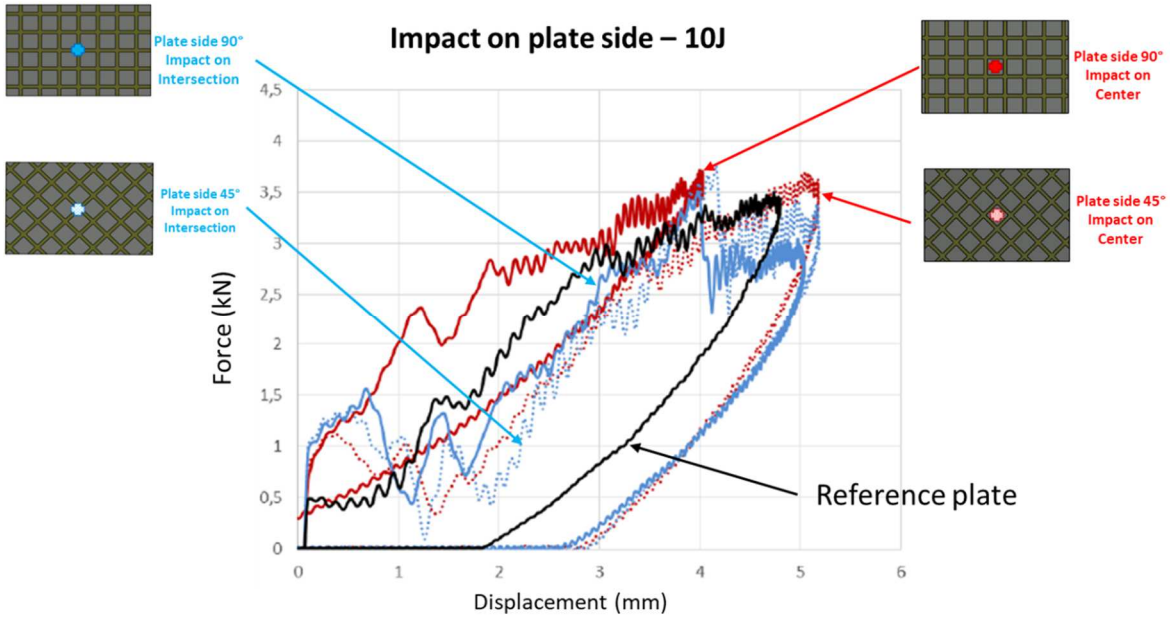

Figure 25. Displacement force curves for an impact at 10 J, plate side.

Force / displacement curves for 15 J impacts.

The displacement force curves for an impact at 15 J are given in Figure 26 for the overmolded grid side, and in Figure 27 for the plate side. Two tests are missing due to an experimental problem but do not change the observed trends. Globally, the behaviour is identical with, of course, the greatest damage when the grid side is impacted. The grid is destroyed in both cases of location of impact and the debonding is complete, or at 80%

when the bottom of the mesh is hit. On the other hand, it is noticeable that, during the impacts on the plate side, the behaviour is very homogeneous and very similar to that of the plate alone.

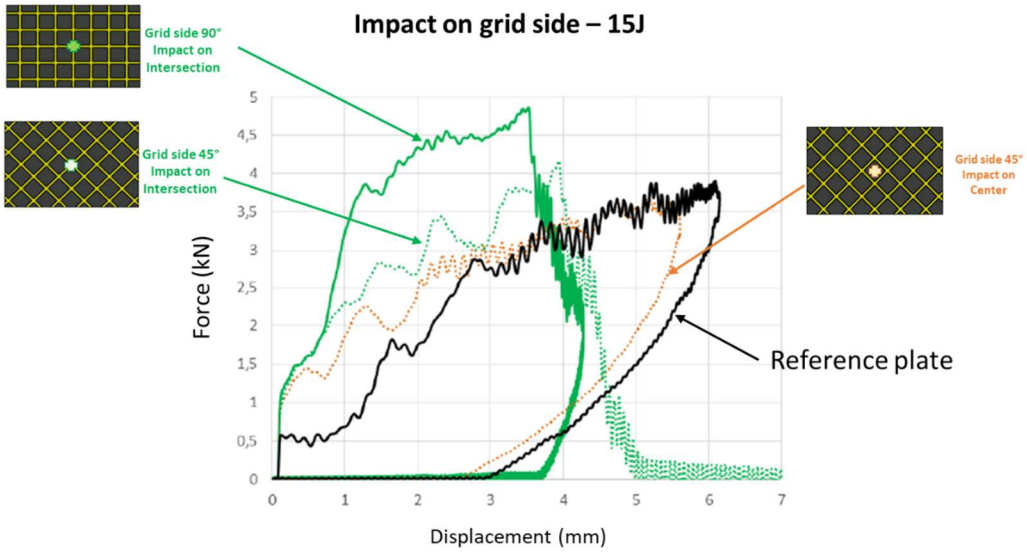

Figure 26. Displacement force curves for an impact at 15 J, overmolded grid side.

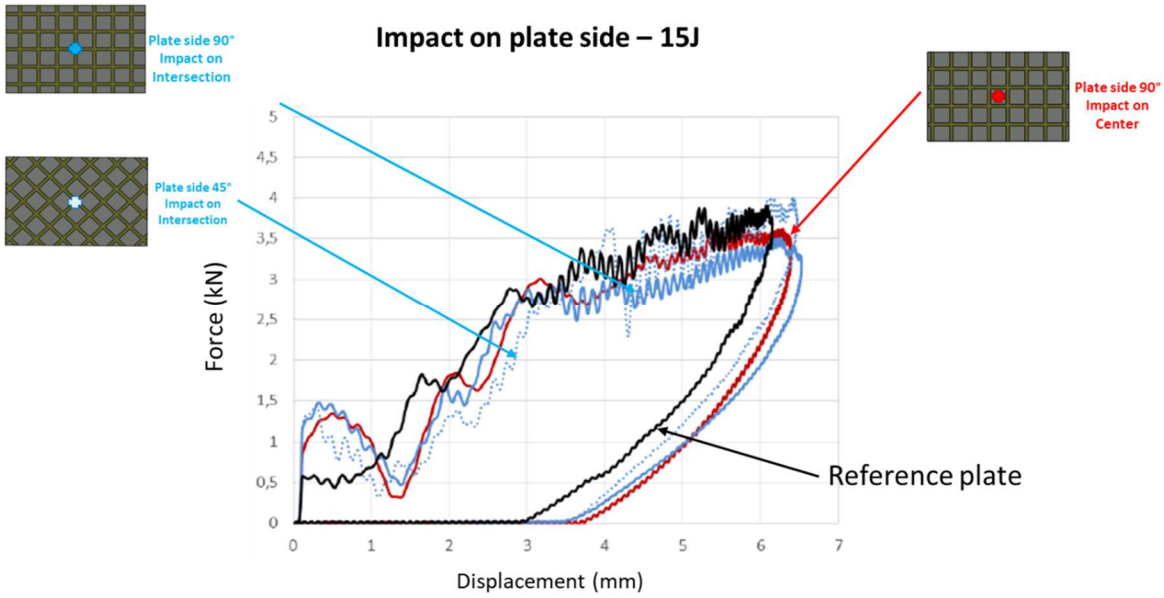

Figure 27. Displacement force curves for an impact at 15 J, plate side.

Tomography analysis of impact patterns

It is very difficult to analyse the effects of impact with qualitative visual observations and force-displacement curves only. So a tomographic analysis was performed. From the tomographic images, it is clear that the grid conditions the damage to the plaque according to the location of the impact. Figure 28 compares the damage at

different impact locations for an energy of 15 J. A non-overmolded plate is also added to the comparison for reference. It can be observed that the extent of the damage undergone by the composite plate is lower for cases B, C and D. For case B, the structure of the overmolded grid seems to have a “shield effect” on the propagation of cracks, which is not observed in case A since the grid is located on the same side as the impact. When the impact is located on the plate side and directly opposite a rib crossing (case C), the damage in the plate is very small compared to what is seen in the reference plate. This can be explained by the flexural stiffness provided by the grid in the impact zone. Finally, in case D, the overmolded grid partially exploded on impact but absolutely no damage was observed, visually or by tomography, on the plate. This result could also be observed for an impact energy of 25 J. When the overmolding grid is directly impacted, it completely dissipates the impact energy and thus protects the composite plate from possible damage.

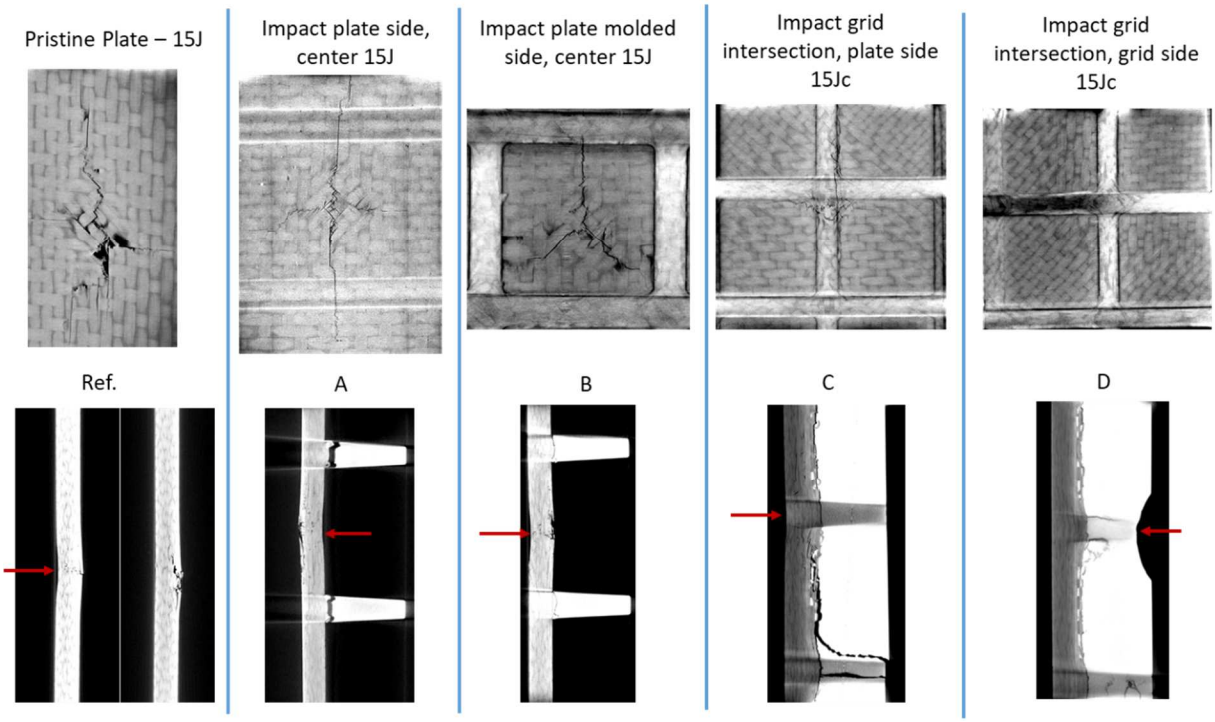

Figure 28. Tomographic images for different impact locations at 15 J.

5. Conclusions

Thermoplastic PEI plates overmolded with a compound based on PPS - short carbon fiber with a ratio of 15% were produced. Preliminary analysis showed that the toughness of the bond between these two materials was rather low, but difficulties in injecting a PEI-based compound, and industrial constraints, argued in its favour. In general, the overmolding process is very complex and expensive but must be justifiable on large series such as

for aircraft seats or through design gains with "net shape" parts. Impact tests were performed at 5, 10 and 15 J following aeronautical standards. These energies are below the BVID of the thermoplastic plate alone. It turned out that, in 80% of the tests, the overmolded grid debonded significantly. It was therefore not necessary to carry out Compression after Impact Compression (CAI) tests [31] to determine the residual strength (i.e. that of the plate alone). From this point of view, the overmolded solution in the studied configuration is not optimal. This behaviour is probably due to poor compatibility of the two thermoplastics, a corrugation defect at the foot of the overmolded rib, many defects at the interface due to the industrial process, or even a sensitivity of the thermoplastics to a speed effect in mode II [14]. It would therefore be advisable to produce new parts with the aim of solving these problems.

6. Acknowledgements

The authors acknowledge Bpifrance Financement for its financial support in the FUI contract N°F1504022M.

7. References

[1] Neveu F, Castanié B, Olivier P. The GAP methodology: A new way to design composite structures. Materials & Design, 172 (2019), Article 107755, https://doi.org/10.1016/j.matdes.2019.107755

[2] Castanie B, Bouvet C, Ginot M. Review of composite sandwich structure in aeronautic applications. Compos Part C Open Access 2020;1:100004. https://doi.org/10.1016/j.jcomc.2020.100004

[3] Susainathan J, Eyma F, De Luycker E, Cantarel A, Castanie B. Experimental investigation of impact behavior of wood-based sandwich structures. Compos Part Appl Sci Manuf 109 (2018), pp 10–19. https://doi.org/10.1016/j.compositesa.2018.02.029.

[4] Lefebure P, Soccard E, Piana M, Guimard JM. Thermoplastic composites technologies for manufacturing nose fuselage structures. SAMPE Journal 2013 49(5), pp. 32-41

[5] Dıaz J, Rubio L. Developments to manufacture structural aeronautical parts in carbon fibre reinforced thermoplastic materials. Journal of Materials Processing Technology 143–144 (2003), pp 342–346.

[6] Magnin P, Andrieu G, Vigueur SM. Full out-of-autoclave thermoplastic welded airframe. JEC Composites Magazine 2018 55(122), pp. 27-29

[7] Pappadà S, Salomi A, Montanaro J, Passaro A, Caruso A, Maffezzoli A. Fabrication of a thermoplastic matrix composite stiffened panel by induction welding. Aerospace Science and Technology 43 (2015), pp. 314-320.

[8] Da Costa AP, Botelho EC, Costa ML, Narita NE, Tarpani JR. A review of welding technologies for thermoplastic composites in aerospace applications. Journal of Aerospace Technology and Management 4(3) (2012), pp. 255-265.

[9] Schell JSU, Guilleminot J, Binetruy C, Krawczak P. Computational and experimental analysis of fusion bonding in thermoplastic composites: Influence of process parameters. J Mater Process Technol 209(11) (2009), pp 5211–5219.

[10] Vieille B, Aucher J, Taleb L. Comparative study on the behavior of woven-ply reinforced thermoplastic or thermosetting laminates under severe environmental conditions. Materials & Design 35 (2012), pp 707-719

[11] Abrate S, Castanié B, Rajapakse YDS. Dynamic Failure of Composite and Sandwich Structures. Springer: Berlin/Heidelberg, Germany, 2013; ISBN 978-94-007-5329-7

[12] Vieille B, Casado VM, Bouvet C. About the impact behavior of woven-ply carbon fiber-reinforced thermoplastic-and thermosetting-composites: a comparative study. Composite structures 101 (2013), pp 9-21

[13] Dubary N, Taconet G, Bouvet C, Vieille B. Influence of temperature on the impact behavior and damage tolerance of hybrid woven-ply thermoplastic laminates for aeronautical applications. Composite Structures 168 (2017), pp 663-674

[14] Perez PG, Bouvet C, Chettah A, Dau F, Ballère L, Peres P. Effect of unstable crack growth on mode II interlaminar fracture toughness of a thermoplastic PEEK composite. Engineering Fracture Mechanics 205 (2019), pp 486-497.

[15] Hufenbach W, Langkamp A, Adam F, Krahl M, Hornig A, Zscheyge M, Modler KH. An integral design and manufacturing concept for crash resistant textile and long-fibre reinforced polypropylene structural components. Procedia Engineering 10 (2011), pp 2086–2091.

[16] Brandenburg SD. Evaluation of overmolded electronic assembly packaging using thermoset and thermoplastic molding. Advancing Microelectronics 34(1) (2007), pp. 24-29.

[17] Zeppenfeld M, Müller B, Heyl S. Influence of Insert Component Position and Geometry on Shrinkage in Thermoplastic Insert Molding. AIP Conference Proceedings 2139 (2019) 030005. https://doi.org/10.1063/1.5121658

[18] Karakaya N, Papila M, Özkoç G. Effects of hot melt adhesives on the interfacial properties of overmolded hybrid structures of polyamide-6 on continuous carbon fiber/epoxy composites. Composites Part A 139 (2020) 106106.

[19] Project "TOAST" https://www.premium-aerotec.com/en/media/press-releases/premium-aerotec-demonstrate-potential-of-a-modern-hybrid-design-for-future-aircraft-lightweight-structures-1/; Accessed 02-15-2021

[20] Green S, Ferfecki FJ, Marburger U. Overmolding of peek compounds for composite aerospace brackets. 2017 CAMX 2017 - Composites and Advanced Materials Expo 2017-December SAMPE JOURNAL, 2018; 54 (3): 22

[21] Valverde MA, Kupfer R, Wollmann T, Kawashita LF, Gude M, Hallett SR. Influence of component design on features and properties in thermoplastic overmolded composites. Composites Part A 132 (2020) 105823

[22] http://www.technimoules.com/ accessed 2021-23-02

[23] https://www.thermoplay.it/fr accessed 2021-23-02

[24] Susainathan J, Eyma F, De Luycker E, Cantarel A, Castanie B. Numerical modeling of impact on wood-based sandwich structures. Mechanics of Advanced Materials and Structures 27 (18) (2020), pp 1583-1598.

[25] E. Morteau, C. Fualdes. Composites @ Airbus, damage tolerance methodology. FAA Work-shop for Composite Damage Tolerance and Maintenance, Chicago IL, 2006. Accessed 05/26/2020 https://www.niar.wichita.edu/niarworkshops/Portals/0/Airbus%20Composites%20-%20Damage%20Tolerance%20Methodolgy%20-%20Fualdes.pdf?ver=2007-05-31-095449-530

[26] Mezeix L, Seman A, Nasir MNM, Aminanda Y, Rivai A, Castanié B, Olivier P, Ali KM. Spring-back simulation of unidirectional carbon/epoxy flat laminate composite manufactured through autoclave process. Composite Structures 124 (2015), pp 196–205.

[27] Fiorina M, Seman A, Castanié B, Ali KM, Schwob C, Mezeix L. Spring-in prediction for carbon/epoxy aerospace composite structure. Composite Structures 168 (2017), pp 739–745

[28] Moretti L, Castanié B, Bernhart G, Olivier P. Characterization and modelling of cure-dependent properties and strains during composites manufacturing. Journal of Composite Materials 54(22) (2020), pp. 3109–3124.

[29] Moretti L, Olivier P, Castanié B, Bernhart G. Experimental study and in-situ FBG monitoring of process-induced strains during autoclave co-curing, co-bonding and secondary bonding of composite laminates. Composites Part A: Applied Science and Manufacturing 142 (2021) 106224.

[30] Susainathan J, Eyma F, De Luycker E, Cantarel A, Castanié B. Experimental investigation of impact behavior of wood-based sandwich structures. Comp Part A 109 (2018), pp 10-19. https://doi.org/10.1016/j.compositesa.2018.02.029

[31] Susainathan J, Eyma F, De Luycker E, Cantarel A, Bouvet C, Castanié B. Experimental investigation of compression and compression after impact of wood-based sandwich structures. Compos Struct 220 (2019), pp 236–49. https://doi.org/10.1016/j.compstruct.2019.03.095.